**NURETH14-139** 

# CFD SIMULATIONS OF BALLOONED REGIONS IN A DAMAGED CORE DURING THE LOCA REFLOOD PHASE

N. Seiler<sup>1</sup>, P. Ruyer<sup>1</sup>, F. Lelong<sup>1</sup>, F. Secondi<sup>1</sup>, M. Gradeck<sup>2</sup>

<sup>1</sup> IRSN/DPAM/SEMCA/LEMAR, CE Cadarache, 13 108 Saint Paul lez Durance, France

<sup>2</sup> LEMTA Nancy University CNRS, Vandœuvre les Nancy, France

#### **Abstract**

This study focuses on the cooling capacity of a damaged PWR reactor core during the reflooding phase of a Loss Of Coolant Accident (LOCA). Downstream the quench front, the core cooling is provided by an over-heated vapour flow carrying water droplets and may impact the ballooned fuel cladding and provide an additional cooling. The present paper will deal with the development of a CFD code to simulate such droplet dispersed flows with the final aim of carrying out sensitivity studies of blockage ratio and length on wall cooling. Adequate closure laws for the momentum and energy balances as well as for the heat transfer at droplet impact and interfacial area transport are given and some simulation results are presented.

### Introduction

This study focuses on the cooling capacity of a damaged PWR reactor core during a Loss Of Coolant Accident (LOCA). During the reflooding phase of such accident, core cooling is provided by an over-heated vapour flow carrying water droplets, which experience break-up and coalescence and may impact the ballooned fuel cladding. Since the temperature of the fuel assemblies is well above the Leidenfrost temperature (> 600°C), the droplet impact regime is the bouncing regime: the strong evaporation flux prevents the droplet from wetting the wall. The heat exchange between the droplet and the hot clad is not negligible and should be considered to evaluate the clad to refrigerant heat transfer. The final aim of the present study is to accurately estimate the cooling capability of ballooned part of a damaged PWR core depending on the blockage ratio, the length of the balloons and on the thermal-hydraulic features of the dispersed droplet two-phase flow through the sub-channels. Indeed, the ballooning of the cladding has an important influence on the dispersed droplet flow and thus on the heat exchange and nuclear core coolability [1].

The French Institut de Radioprotection et de Sûreté Nucléaire (IRSN) has launched in 2006 a wide Research and Development Program on LOCA on this issue. The simulation part of this program deals with the adaptation of the CFD code Neptune\_CFD (mainly devoted to bubbly and separated-phase flows) to the simulations of dispersed droplet two-phase flows involving steep thermal gradients and thus heat transfers. The final goal is to develop an operational tool enabling sensitivity simulations to droplet diameters and relative velocities, fuel power, ratio of ballooning etc which would, on one hand, study the cooling capability at CFD scale and, on the other hand, provide adequate closure laws for the study of reflooding phase in such LOCA conditions at a component scale.

The present paper will first present the adequate closure laws of the two-fluid model at the basis of Neptune\_CFD. One focuses on both momentum and energy balances. Furthermore, the conclusions of an experimental study aiming at measuring heat transfer at droplet impact, and the associated validated heat transfer model, adapted to CFD scale, will be described. In addition, an interfacial area transport equation is considered to follow the droplet diameter evolution according to thermal (evaporation/condensation) and dynamical phenomena (break-up/coalescence).

Finally, simulation results of steam-droplet flows throughout sub-channels involving ballooned rods are analyzed, conclusions and perspectives are drawn.

## 1. Dispersed droplet flow closure laws

Neptune\_CFD code is a Euler-Euler three dimensional two-fluid code developed more especially for nuclear reactor applications and mainly devoted to bubbly and separate-phase flows. This local three-dimensional module is based on the classical two-fluid one pressure approach, including mass, momentum and energy balances for each phase[2], [3]. Firstly, the code has been adapted to droplet flows, implementing adequate closure laws.

### 1.1 Momentum Source Terms

In the momentum balance equation for phase k, the interfacial momentum transfer  $M_{ki}$  from phase k to the interface between droplet and vapour  $[kg/m^2/s^2]$  needs to be modelled:

$$\frac{\partial(\alpha_k \rho_k \vec{v}_k)}{\partial t} = \dots \Sigma \vec{M}_{k,i} \tag{1}$$

where  $\alpha$ ,  $\rho$ , v stand for the volumetric fraction, density and velocity of phase k, index k taking l value for liquid droplet phase and g for vapour gaseous phase.  $M_{ki}$  is modelled as the averaged sum of the forces that govern droplet motion. The different forces are analyzed in the following sections.

## 1.1.1 Drag and Added Mass Forces

In LOCA conditions eg [4,5], the typical droplet diameters range is from few micrometers to some millimeters for which surface tension force confers a spherical shape. The liquid volumetric fraction ranges between  $10^{-4}$  and  $10^{-2}$  which induces dilute flow of particles, *i.e.* low rate of collision.

It has been checked that the drag and added mass forces expressions existing in Neptune\_CFD [2] are adapted to the droplet case, but the added mass force is negligible in case of droplet flow. These expressions are valid for isolated (diluted flow) spherical inclusions which actually correspond to flow features

### 1.1.2 Lift Force

A particle moving in a fluid having a non-uniform velocity experiences a lateral lift force due to two different mechanisms: 'slip-spin' motion (or Magnus effect, when a rotating sphere moves parallel to the streamlines) and 'slip shear' motion (when the sphere moves through a viscous fluid in shear flow). Regardless these two effects, The Auton's expression of the lift force is commonly used for bubbly flow [6]. Nevertheless, in case of droplet flow, this force is overestimated leading to an incorrect droplet distribution within the flow [7]. It is commonly

accepted in the literature that the lift force depends on the Reynolds number based on the particle motion  $\text{Re}_p$  ( $\text{Re}_p = \rho_g v_r d/\mu_g$  where  $v_r$  stands for the relative velocity  $v_r = v_l - v_g$  and  $\mu$  for the viscosity) and the local shear stress of the surrounding flow. Based on Saffman's expression for lift coefficient [8], the average contribution of lift on  $M_{ki}$ , namely  $M_i^L$ , reads:

$$\vec{M}_{l}^{L} = \frac{\alpha_{l}}{d} \sqrt{\rho_{g} \mu_{g} \frac{dv_{g}}{dr} (\vec{v}_{g} - \vec{v}_{l}) \vec{n}}$$
(2)

with d the droplet diameter,  $\vec{n}$  the unity vector having a direction perpendicular to the main flow and r the corresponding coordinate. However, the Auton and Saffman's expressions are only valid for smaller Reynolds numbers than that encounter in LOCA conditions. Recent DNS studies [9] [10] show that the lift coefficient at high Reynolds numbers is lower and could eventually drop to zero and change of sign for given values of the shear stress and Re number. A new expression from these DNS studies is currently tested in Neptune\_CFD and would, at term, replace the Saffman's expression.

#### 1.1.3 Contribution of turbulence forces

In a dispersed droplet flow, both the continuous (vapour) and the dispersed (droplets) phases contribute to the turbulent regime. Their turbulent regimes are somehow coupled. Droplets are subjected to turbulent fluctuations that increase their diffusion and mixing with the vapour phase. At the same time, the presence of the dispersed phase modifies the turbulence of the continuous phase taken into account through the k- $\varepsilon$  model [11]. The main disadvantage of this model is that it is not adequate for highly anisotropic or rotating flow, as it could occur in ballooned regions. Hinze-Tchen's particle tracking fluid theory [12], which is used to model the dispersed phase turbulence, is a local equilibrium model with a simplified approach applicable to dilute flows. Some algebraic formulations are used to link the dispersed particle turbulence to the gas flow turbulence via inertial drag expression. It states that the particle turbulence fluctuation is weaker than the fluid turbulent fluctuation and it decreases with the increase of droplets size. These hypothesis could not fit the targeted flow features especially if we refer to the recent works of Zhou [13] that has shown that in some cases and regions the particles fluctuation could be stronger than the fluid one. Alternative to Tchen's model considers additional transport equations to estimate the droplets mean fluctuating motion. Moreover, the turbulent reverse coupling model [2] has to be taken into account for the modification of the turbulent viscosity of the continuous phase due to the presence of the dispersed phase.

Finally the turbulent contribution of the interfacial momentum transfer gathers the fluctuating part of the drag and added mass forces as well as the fluctuating pressure term due to the correlation between the particles distribution and the carrier phase stress tensor.

### 1.1.4 Thrust force

Ganic et Rohsenow [14] observed in dispersed flow film boiling regime an additional force associated with drop motion. Indeed, because of the temperature gradient in the thermal boundary layer, the side of the droplet closer to the wall evaporates at a higher rate and vapour is produced at higher velocity than on the cold side. This results in a reaction or thrust force, which tends to prevent the deposition of droplet on the wall [15]. The velocity of the evaporating vapour is estimated by dividing the evaporated mass flux by the local vapour density. Within the framework of the IRSN Research and Development Program on LOCA, an experimental study followed by modelling work was achieved in 2010. It provides a model for the heat flux removed

by the droplet impact on the wall. From this expression, the evaporated mass flux could be derived and the thrust force expression is foreseen to be implemented into the code Nepttune\_CFD in 2011.

# 1.2 Enthalpy Source Terms

Interfacial heat and mass transfer plays a major role in the energy and mass balance equations of both phases. The global heat transfer at the droplet interface between the vapour phase and the liquid droplet is represented by a double boundary layers model (figure 1). It is assumed that the interface between the vapour and the liquid is at the thermodynamical equilibrium and remains thus at saturation temperature.

The heat transfers through the liquid and vapour boundary layers are modelled using empirical correlations. They induce either cooling down/heating up or evaporation/condensation.

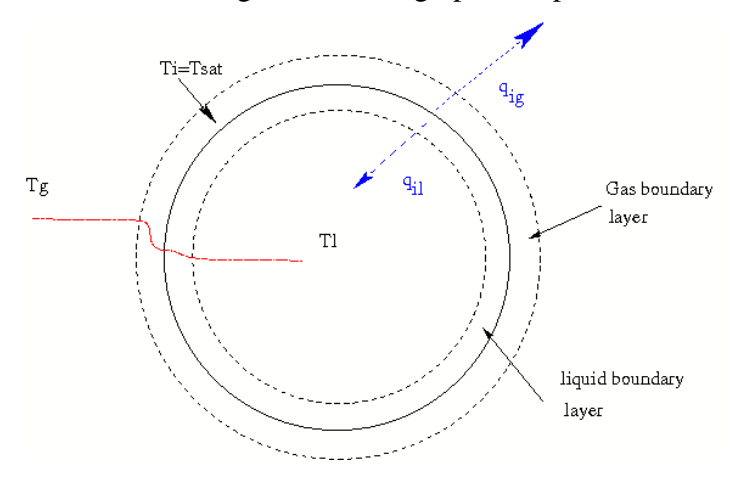


Figure 1 : Double boundary layer model at the droplet interface.

## 1.2.1 Liquid side interfacial heat transfer

The most basic model for heat transfer inside a spherical inclusion is the relaxation model [2,3]. Its name stands for the return to saturation conditions in a given relaxation time. This time is usually specified by the code user. Such model could be used for droplet inclusion, but more realistic model must be used to evaluate this time.

# $\chi$ model:

The external flow outside the droplet may induce, owing to shear stress, an internal convection (spherical Hill vortex pattern). Fine estimation of thermal heat transfer would require a resolution of the flow inside the drop, e.g. [16]. Abramzon et Sahzin [17] proposed an approximation resolution thanks to a model involving a factor  $\chi$  (varying from 1 to 2.72):

$$\chi = 1.86 + 0.86 \tanh[2.245 \log_{10} \frac{Pe_i}{30}]$$
(3)

where the liquid Peclet number is given by  $Pe_l = V_{\max} d / \kappa_l$  with  $\kappa_l$  the liquid thermal diffusivity and  $V_{max}$  the maximal velocity of the flow at the interface:

$$V_{\text{max}} = \frac{v_r}{32} \frac{\mu_g}{\mu_l} \text{Re}_p C_F (\text{Re}_p)$$
 (4)

with  $C_F(Re_p)$  the shear coefficient given by:

$$C_F(\text{Re}_P) = \frac{12.69}{\text{Re}_P^{2/3}(1+B_M)}$$
 (5)

This last equation is valid for  $10 < Re_p < 100$  and  $B_M$  is the Spalding number associated to the diffusion effect of the vapour through the air and consequent limitation of the mass transfer at the interface. The heat flux at the droplet interface is  $[in \ W/m^2]^1$ :

$$\Phi_{il} = \chi k_i [T_{sat} - T_i] \frac{10}{d} \tag{6}$$

with  $k_l$  the liquid conductivity and d the droplet diameter. Finally, the volumetric heat flux from the interface to the liquid  $[W/m^3]$  is given by equation (7):

$$q_{ii} = \alpha_i [T_{sai} - T_i] \frac{60 \chi k_i}{d^2} \tag{7}$$

#### Hendou's model:

The heat transfer coefficient inside the liquid boundary layer is modelled by empirical correlations that depend on the flow regime inside the droplet [18]. In case of droplets with laminar recirculation:

$$Nu_{I} = 2.567 + 0.794 \operatorname{Re}_{P,liq}^{1/2} \operatorname{Pr}_{P,liq}^{1/3}$$
 (8)

with  $Re_{P,liq} = \rho_l v_l d/\mu_l$  and  $Pr_{P,liq} = \mu_l C_{p,l}/k_l$ . In case of droplets with turbulent recirculation:

$$Nu_{I} = 0.351 + 0.381 \operatorname{Re}_{P,liq}^{1/2} \operatorname{Pr}_{P,liq}^{1/3}$$
(9)

Finally, the volumetric heat flux from the interface to the liquid  $[W/m^3]$  is:

$$q_{ii} = \alpha_{i} N u_{i} \frac{6k_{i}}{d^{2}} [T_{sai} - T_{i}]$$
 (10)

The  $q_{il}$  given by eq. (10) and (7) differ of  $Nu/(10 \chi)$ .

# 1.2.2 <u>Vapour side interfacial heat transfer</u>

### Ranz-Marshall's model:

The heat transfer due to the flow around a sphere is usually given by the Ranz-Marshall's correlation [2]:

$$Nu_g = 2. + 0.6 \operatorname{Re}_{P,g}^{1/2} \operatorname{Pr}_{P,g}^{1/3}$$
 (11)

and the volumetric heat flux from the interface to the vapour  $[W/m^3]$  is:

$$q_{ig} = \alpha_i N u_g \frac{6k_{gl}}{d^2} [T_{sat} - T_g]$$
(12)

# Lee's model:

The Lee model takes into account a kinetic limitation due to evaporation. It has been shown that, at high evaporation rates, the evaporation reduces the convective heat transfer from vapour to the droplet [19,20]. Indeed the vapour mass flux, leaving the surface of the droplet, flows countercurrent to the heat flux. Lee *et al.* [21] corrected the average Nusselt number by the blowing factor B:

<sup>&</sup>lt;sup>1</sup> If a linear temperature profile is supposed inside the droplet, it comes  $T_i$ =0.5 ( $T_{sat}$ + $T_{(droplet \, center)}$ ) and thus the heat flux (6) is 2.5 times less important.

$$Nu_{g}(1+B) = 2. + 0.74 \operatorname{Re}_{p,vap}^{1/2} \operatorname{Pr}_{p,vap}^{1/3}$$
(13)

where B is the mass transfer number defined as:

$$B = \frac{\left[h_{s}\left(T_{s}\right) - h_{l}\left(T_{l}\right)\right]}{\left[h_{s}\left(T_{l}\right) - h_{l}\left(T_{l}\right)\right]}$$
(14)

with  $h_k$  the enthalpy of the phase k. The volumetric heat flux from the interface to the vapour is obtained by eq. (12).

## 2. Direct Contact Heat Transfer

During the reflood phase of a LOCA, wall temperatures are above 500°C which is much higher than the Leidenfrost temperature of liquid water. In this particular impact regime, a thin vapour layer appears between the droplets and the heated slab so that direct contact with the hot solid is avoided. For low Weber number, characteristic of LOCA conditions, the surface energy is high enough compared to the kinetic energy to permit the rebound of the droplet which recovers its initial shape without breaking up. The generated vapour layer thermally insulates the droplet and minimizes the loss of heat from the surface at the impact.

There is a lack of knowledge on the heat exchanged at the droplet impact on hot ballooned cladding. According to Andreani [5], this heat transfer is of the same order of magnitude than the convective heat transfer and should therefore be considered. An experimental set-up has been built to measure the heat removed by a single droplet impact while catching simultaneously the dynamical deformation over the hot wall. The experiments in ambient conditions are performed with very small droplets (80-300 µm) injected at 30°C at high frequency using a purpose-designed piezoelectric nozzle that allows to adjust the droplet frequency, velocity and size at the injection. The target wall is a very thin disk of Nickel (500µm thickness) heated beforehand around 600°C by an electromagnetic inductor device. At initial time, heating is shutdown and the heat flux removed from the wall by the impinging droplets (front face of the disk) is deduced by post-processing the temperature field (measured in the rear face of the disk using an infrared camera) thanks to a specifically developed semi-analytical inverse heat conduction model [22] [23].

A mechanistic approach is proposed for the modelling of the heat transfer between the droplet and the heated wall [24]. This model is based on combined dynamical and thermal considerations. The droplet dynamics is considered through a spring's analogy in order to evaluate the dynamics of the spreading diameter and the duration of the droplet/wall thermal interaction, called resident time. The thickness of the vapour cushion beneath the droplet is determined by balancing both momentum and heat and mass transfer within it. These results are validated against experimental data.

The energy  $\Phi$  [J] removed by the droplet from the heated wall has been expressed by F. Lelong [24] and depends on droplet features, Weber and Reynolds numbers and wall temperature. From this expression, the average heat flux between droplets and the heated wall is derived:

$$\Phi_{G} = \alpha_{g} \frac{6V_{n}}{\pi d^{3}} \Phi \tag{16}$$

It is implemented into the Neptune\_CFD code as an additional heat transfer This heat transfer is considered in the mass or energy balance equations according to the mechanistic model [24]. It actually corresponds to the sum of convective heat transfer due to strong vapour flow, heating up of a tiny part of the droplet and of its subsequent evaporation. Thus source terms to the phasic mass and enthalpy balance equations have been derived according to this decomposition. We

therefore introduce the ratio r, defined as  $r = h_{LV} / [h_{LV} + C_{P,l} (T_{sat} - T_l)]$ , to evaluate the evaporation part. Thus, the heat transfer due to droplet impact and leading to additional droplet evaporation is modeled as a volumetric source term  $TS_{\Gamma}$  in the cells of volume  $V_{cell}$  having wall as boundary over a surface  $S_{wall}$ . It reads:

$$TS_{\Gamma} = \Phi_{G} \times \frac{S_{walli}}{V_{coll} h_{IV}} \times r \tag{17}$$

$$TS_{H_t} = \Phi_G \times \frac{C_{p,L}}{h_L} \times (1-r)$$

$$\tag{18}$$

with  $h_L$  the liquid convective exchange coefficient derived from eq. (7) or (10).

In the determination of this direct contact heat transfer, the radiative heat transfer between the wall and the droplet is negligible [24]. However, considering the dispersed droplet flow topology encountered in LOCA conditions, the medium is non thermally homogeneous, absorbing, anisotropically scattering, emitting and non grey. The radiative heat transfer could not be neglected [15] and a choice of an enough accurate but low time consuming method to compute the radiative heat transfer equation is underway at IRSN [30].

## 3. Interfacial Area Equation

Due to the importance of surfacic transfers at the droplet interface, the prediction of the volumetric interfacial area ( $a_i \ [m^{-1}]$ ) is essential. This implies to model its temporal and spatial evolution (due to droplet condensation/evaporation or dynamical phenomena). As, some inaccuracies remain in the correlations giving the heat exchanges (eq. (7), (10), (12)) and no data of spatial droplet diameter distribution are available in case of LOCA, the development of a monodispersion model, i.e. single droplet size equal to the Sauter diameter in the whole domain, has been preferred to a polydispersion model due to the lack of an accurate knowledge on boundary conditions. The transport equation of the interfacial area is given by equation (19)  $[m^{-1} \ s^{-1}]$  [25]:

$$\frac{\partial a_i}{\partial t} + \nabla \cdot (a_i \vec{v}_i) = \frac{2}{3} \left( \frac{a_i}{\alpha_i \rho_i} \right) \left[ \Gamma_i - \alpha_i \frac{\partial \rho_i}{\partial t} \right] + TS_{ai,co} + TS_{ai,br}$$
(19)

In this equation, the first term on the RHS represents the change in volume of the droplets (due to evaporation/condensation, compressibility); the last two terms are break-up and coalescence source terms.

#### 3.1 Phase Change

The interfacial mass transfer term  $\Gamma_l$  is related to the interfacial heat transfers on vapour and liquid sides. An additional term is considered for the near wall evaporation of droplets impinging. It reads:

$$\Gamma_{l} = \frac{\left(-q_{ig} + q_{il}\right)}{h_{LV}} + TS_{\Gamma} \tag{20}$$

#### 3.2 Coalescence

The coalescence decreases the number of droplets and increases the mean Sauter droplet diameter ( $d_{Sauter} = 6\alpha/a_i$  in case of monodispersion). It has been evaluated by O'Rourke [26]:

$$TS_{ai,co} = 12\pi \left(\frac{\alpha_i}{a_i}\right)^2 (n \ f_{col}\eta_{co})$$
 (21)

with n the droplet density number,  $f_{col}$  the droplet collision frequency and  $\eta_{co}$  the coalescence efficiency. Under the assumption of monodispersion, the density number can be written:

$$n = \frac{1}{36} \frac{a_i^3}{\alpha_i^2} \tag{22}$$

The collision frequency could be derived from the vapour turbulence which causes eddying motions, enabling droplets to collide. Thus the root-mean-square velocity between two particles  $(v_{rel,d})$  can be written as a function of droplet diameter and turbulent dissipation ( $\varepsilon$ ), the constant being evaluated by Aly [27]:

$$f_{col} = n\pi d^2 v_{rel,d} = \sqrt{8.2} \left( 6\varepsilon \frac{\rho_l}{\rho_s} \right)^{1/3} a_i^{2/3}$$
 (23)

The collision efficiency is given by:

$$\eta_{co} = \min\left(1, \frac{3.12}{We}\right) \tag{24}$$

Therefore:

$$TS_{ai,co} = 12\pi \left(\frac{\rho_l}{\rho_g}\right)^{1/3} \frac{\sqrt{8.2}\varepsilon^{1/3}}{6^{5/3}} a_i^{5/3} \alpha^{1/3} \eta_{co}$$
 (25)

## 3.3 Break-up

The break-up of a droplet depends on the balance between the external shear stresses that attempt to break up the droplet and the surface tension that resists to this deformation. Among the different possible mechanisms leading to droplet break-up, only the turbulent induced break-up is considered in the following because it is predominant in LOCA conditions. The break-up source term in the equation (19) is a function of the droplet density number, the break-up frequency  $f_{br}$  and of the break-up efficiency  $\eta_{br}$  [28].

$$TS_{ai,br} = 12\pi \left(\frac{\alpha_l}{a_i}\right)^2 (n \ f_{br}\eta_{br}) = 12\pi \left(\frac{\alpha_l}{a_i}\right)^2 (n \left[\left(\frac{d}{d_{cr}}\right)^3 - 1\right] f_{br}$$
 (26)

where  $d_{cr}$  is the critical droplet diameter beyond which break-up takes place. It reads, e.g. [29]:

$$d_{cr} = \left[\frac{We_{cr}\sigma}{8.2\rho_{g}}\right]^{3/5} \left(\frac{\rho_{l}}{\rho_{g}}\right)^{-2/5} \varepsilon^{-2/5}$$
(27)

where the critical Weber number Wear depends on the droplet Reynolds number:

$$\begin{cases} We_{cr} = 5.5 \left( \frac{24}{\text{Re}_p} + \frac{20.18}{\text{Re}_p^{0.615}} - \frac{16}{\text{Re}_p^{2/3}} \right) & 200 < \text{Re}_p < 2000 \\ We_{cr} = 5.468 & \text{Re}_p > 2000 \end{cases}$$
(28)

The droplet break-up frequency is estimated by the time scale of the turbulence:

$$1/f_{br} = \left(\frac{\rho_g}{\rho_I}\right)^{1/3} \frac{d^{2/3}}{\sqrt{8.2}\varepsilon^{1/3}}$$
 (29)

Therefore:

$$TS_{ai,br} = 12 \left( \frac{\rho_i}{\rho_g} \right)^{1/3} \frac{\sqrt{8.2} \varepsilon^{1/3}}{6^{8/3}} a_i^{5/3} \alpha \left[ \left( \frac{d}{d_{cr}} \right)^3 - 1 \right]$$
 (30)

#### 4. Simulation Results

As no local experimental data is available until now, in the literature, simulation results obtained with the Neptune\_CFD code are presented in this section. The geometry of the calculation domain is first described and the main results are presented focussing on the dynamics of droplets and on the evaluation of heat transfers.

#### 4.1 Geometries and flow features

The geometry consists of a part of the core subchannels (figure 2). A subchannel is defined as the fluid domain between eight adjacent fuel rods. Three adjacent core subchannels are considered in the present geometry: the first and second sub-channels are constricted due to the ballooning of four adjacent fuel rods, while the third sub-channel has a constant section along its whole length. The ratio of ballooning is defined as  $(1-S_{bal}/S_{nbal})$  with  $S_{bal}$  the fluid cross section in the ballooned region and  $S_{nbal}$  the fluid section in the non-ballooned region. Different ratio of ballooning are studied (28%, 61% and 90 %). For ballooning ratio more than 61 %, the contact between adjacent rods avoid cross flows between sub-channels over the balloon length. The length of the present geometry is about the typical distance between two horizontal grids (350 mm) and the length of the balloons is 196 mm.

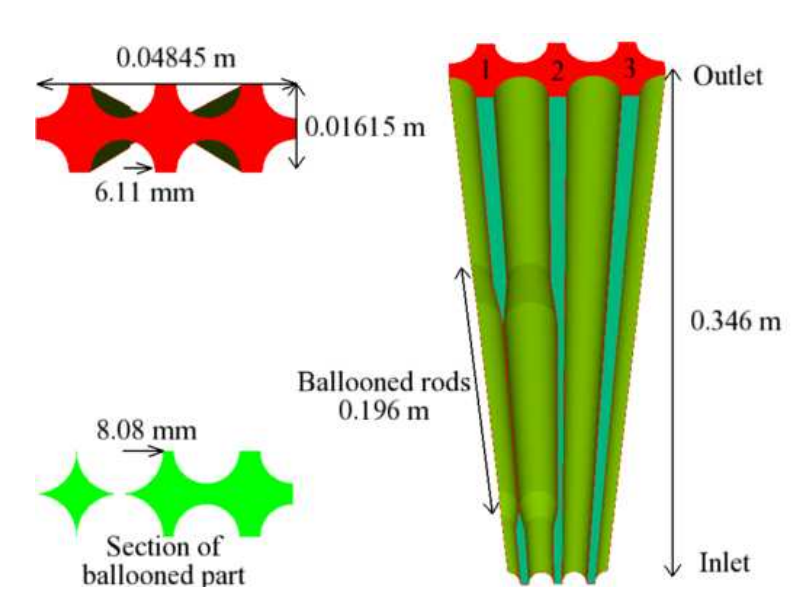


Figure 2: Studied geometry with four rods ballooned (subchannel 1).

Liquid and vapour velocities ( $v_l$  and  $v_g$ ), temperatures ( $T_l$  and  $T_g$ ), and volumetric fractions, representative of a LOCA ( $v_l$ :=1-5 m/s,  $v_g$ =1-10 m/s,  $\alpha_l$ =10<sup>-4</sup>-10<sup>-2</sup>,  $T_l$  around saturation,  $T_v$  from

saturation to 800 °C), are imposed as boundary conditions at the bottom inlet of the domain. Symmetry boundary conditions are considered on the open vertical surfaces between subchannels. Adiabatic, imposed heat flux or temperature can be used as wall boundary conditions. There is no wall conduction simulated up to now. Outlet boundary condition is an imposed level of pressure. The convergence of the different simulations is checked.

## 4.2 Dynamics

The thermal heat transfer is greatly influenced by the dynamical two-phase flow behaviour and especially the droplet spatial distribution within the geometry. That underlines the need of an accurate prediction of the two-phase flow dynamics. The effect of each force has been analysed independently; the drag, the turbulent and the lift (already discussed) influence the flow.

The flow of each phase is deviated towards the bypass channel (third subchannel) due to the variation of horizontal flow sections in the first and second subchannels. Downstream the ballooned region, vapour turns back in the first subchannel whereas, due to their inertia, droplets do not follow the same path. Some droplets bounce on the wall. To interpret the inertial behaviour of droplets, a Stokes number can be defined as the ratio of the relaxation time of the droplets to the characteristic time of the flow around the obstacle (which is the change of section due to the balloon),  $D_{ob}$  being the obstacle dimension:

$$St = \frac{V_g}{D_{ob}} \frac{\rho_l}{\rho_g} \frac{4d}{3C_D V_{rel}}$$
(31)

if St>1, which is the most frequent cases in LOCA conditions, the droplet trajectories do not follow the vapour flow deviation: they are in a regime of inertia. But if St<1, droplets follow the vapour streamlines closely. In Figure 3, the liquid and vapour trajectories in case of 61 % of ballooning and St=205.5 are shown.

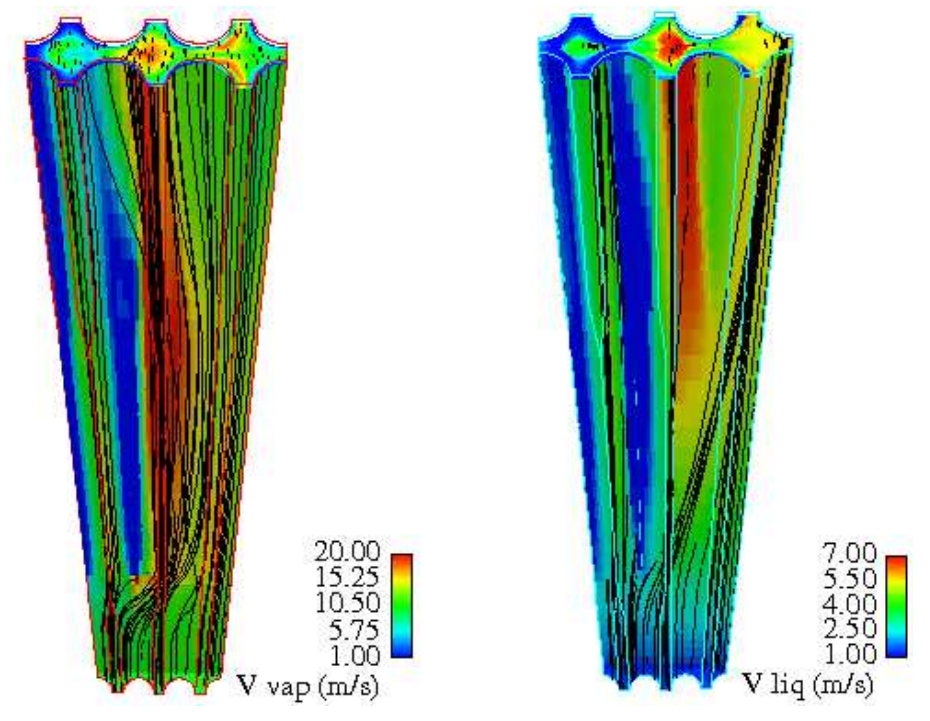


Figure 3: Vapour and liquid velocity fields and trajectories (61% of ballooning ratio, inlet conditions:  $d=5\ 10^{-4}$ m,  $v_l=1$ m/s,  $v_g=10$  m/s St=205.5,  $T_l=372.15$  K,  $T_g=573.15$  K).

Figure 4 illustrates results obtained with different flow features  $d=5\ 10^{-5}$ m (St=20.55) or d= $10^{-3}$ m (St=410.56). The liquid is deviated towards the right by the ballooned region. As St number increases, the deviation downstream is more important which modifies the droplet spatial distribution as it can be seen on the volumetric fraction liquid field at the outlet top boundary of the domain.

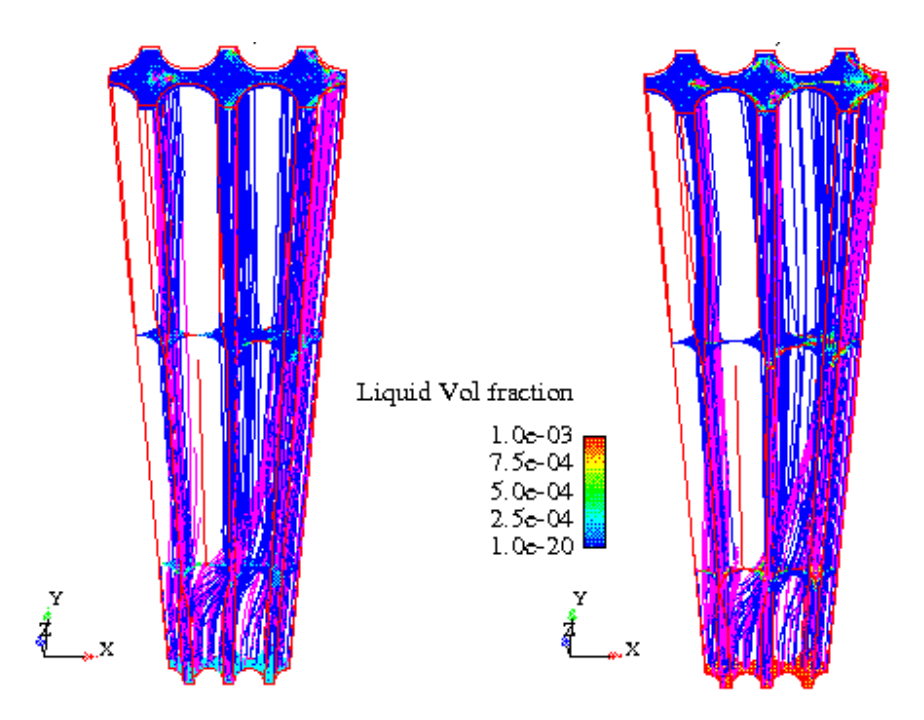


Figure 4 : Liquid trajectories and volumetric fraction for different flow features (on the left : d=5  $10^{-5}$  m, St=20.55, on the right = d= $10^{-3}$ m, St=410.56; 61% of ballooning ratio, inlet conditions:  $v_l$ =1m/s,  $v_g$ =10 m/s,  $T_l$ =372.15 K,  $T_v$ =573.15 K,  $\alpha_l$ =0.01).

# 4.3 Thermics

Sensitivity studies have been carried out on interfacial heat transfer models. The liquid temperature reaches the saturation temperature downstream the inlet (at a location depending on the chosen model  $q_{il}$ ). From the  $\chi$  and Hendou models, relaxations time could be derived and compared; they are relatively similar. As the  $\chi$  model is derived from a more mechanistical approach, it is preferred. The vapour temperature decreases (from 573K at the inlet) non uniformly in the various subchannels but does not reach  $T_{sat}$ . Lee's model leads to lower vapour cooling down than Ranz's model. The former is more adapted to droplet flow because it handles the diffusion limitation owing to the vapour mass flux leaving the interface. A part of the liquid is evaporated and consequently the flow accelerates and the liquid diameter slightly decreases (1-2 % when break-up and coalescence are not considered).

Figure 5 gives the droplet diameter evolution within the domain. In this case, the initial droplet diameter is  $50 \mu m$ . It first uniformly decreases due to evaporation resulting from interfacial heat transfers. Upstream the section restriction (90% of ballooning) droplets get accumulate or are deviated towards the bypass. Coalescence is important at the center of the subchannels and where droplets accumulate. The droplet diameter increases up to  $370 \mu m$  upstream the restriction, in the

bypass and downstream the balloon where flow recirculation occurs. On the contrary, break-up effect is mainly dominated by coalescence, and acts significantly only near the wall where turbulent intensity is larger.

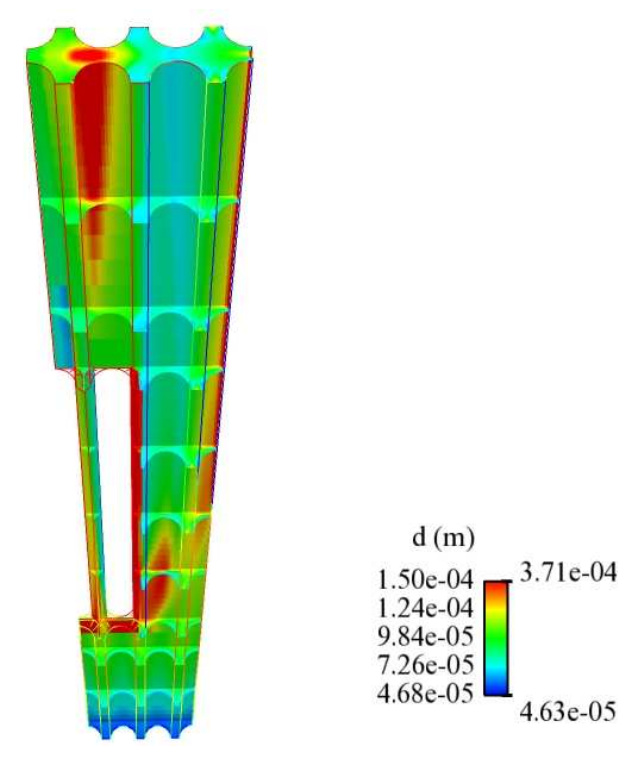


Figure 5 : droplet diameter field (90% of ballooning ratio: no cross-flows, inlet conditions :  $v_l$ =5m/s,  $v_g$ =10m/s,  $T_l$ =353.15 K,  $T_v$ =573.15 K,  $\alpha_l$ =0.001).

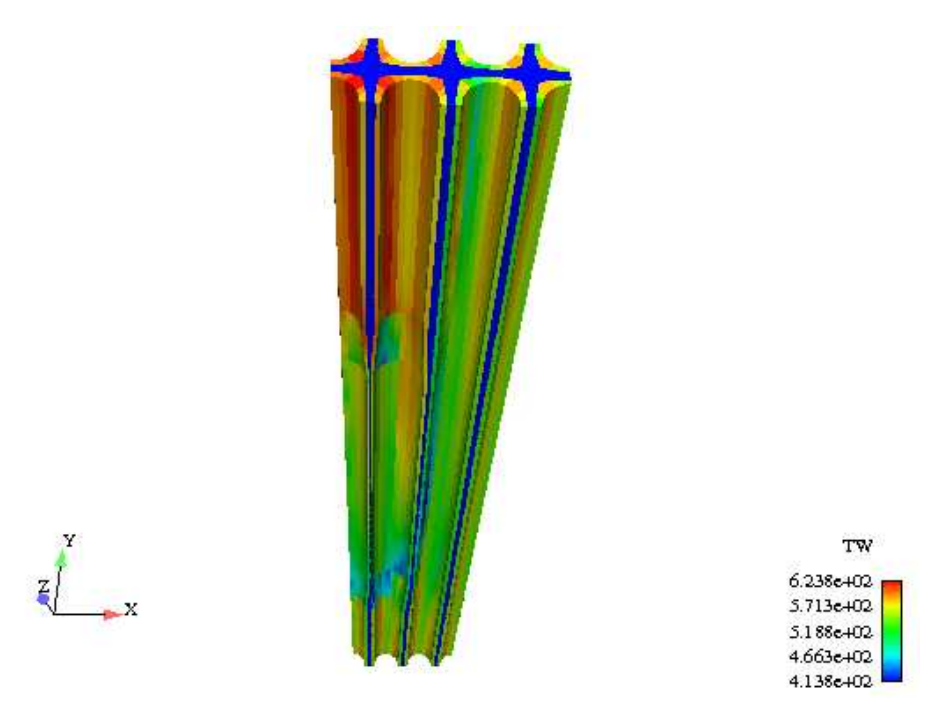


Figure 6: Wall temperature field (61% of ballooning, inlet conditions:  $v_l$ =1m/s,  $v_g$ =5 m/s,  $T_l$ =353.15K,  $T_v$ =473.15 K,  $\alpha_l$ =0.01,  $\Phi_w$ =6000Wm<sup>-2</sup>). Blue cells are not in contact with walls.

Finally, some simulations with imposed wall heat flux or temperature have been performed. Figure 6 illustrated the wall temperature obtained with a constant wall heat flux of 6000Wm<sup>-2</sup>. At the lower part of the ballooned region in the second and third subchannels the heat flux removed by droplet impact reaches a maximum and the lowest wall temperatures are observed (450K). The rate of evaporation is high at this location. Then, in the balloon region, the wall temperature increases again and reaches (500K). Finally, downstream the balloon in the left hand side subchannel, the liquid volumetric fraction is low near the wall (mainly due to deviation and concentration in the centre of the subchannel) and the flow is thus not able to extract a lot of energy from the wall which heats up to 620 K.

# 5. Conclusion and Perspective

This paper summarizes the work achieved within the framework of the Research and Development Program on LOCA at IRSN. The goal is to accurately estimate the cooling capability of ballooned part of a damaged PWR core depending on the blockage ratio, the length of the balloons and on the thermal-hydraulic characteristics of the dispersed droplet two-phase flow entering the subchannels. The program consists in investigating the main thermal transfer modes and in adapting the Neptune\_CFD code to the simulation of droplet dispersed flow.

The dynamical and thermal closure laws adequate for small spherical liquid droplets within overheated vapour have been implemented into the code. A mechanistical model for heat transfer due to direct droplet impact on hot ballooned cladding has also been developed and validated on separated effect tests before being implemented. Finally, in order to have a good prediction of the heat exchanged through the droplets interface, a transport equation of the interfacial area has been considered and its source terms related to phase change, coalescence and break-up have been derived and implemented.

Finally, several sensitivity studies involving various flow features, ballooning ratios, wall heating have been performed. The liquid droplets tend to be deviated towards the bypass depending on their diameters and relative velocity with the carrier phase. Some of them impact at the beginning of the ballooned region and some other penetrate inside it. The droplets are evaporated (in overheated vapour) that contributes to the flow acceleration. The droplets could also experience coalescence, where they accumulate, and break-up near the walls. Downstream the balloon, a flow recirculation is expected. These flow features influence the wall heat transfer. Better cooling is expected upstream the balloon thanks to higher droplet impact rate, but the thermal heat transfer could be less efficient downstream the balloon.

However some tasks are still underway to improve the Neptune\_CFD code applied to droplet dispersed flow. Works are in progress on thurst and lift forces, as well as on turbulence modeling ( $R_{ij}$ - $\varepsilon$ ,  $q_2$ - $q_{12}$  models [7]) and on radiative heat flux. Indeed, from our first evaluations, the radiative heat flux in such a grey diffusing absorbing medium (either optically thin or thick depending on the droplet features) is of the order of magnitude of the convective heat flux and has to be taken into account in Neptune\_CFD, which does not handle any radiative heat flux models [30]. A conductive heat transfer inside the clad could also be envisaged. Moreover, following a R&D program devoted to LOCA, called CYCLADES, each phenomenon is, as much as possible, validated independently on separated effects tests such as droplet impact on hot wall, radiative heat transfer through a ramp spray. Finally, the code results will be validated against a integral experiment with local two-phase flow measurements which it foreseen to be performed at IRSN within the framework of the CYCLADES program.

#### 6. References

- [1] C. Grandjean, "Coolability of blocked regions in a rod bundle after ballooning under LOCA conditions: main findings from a review of past experimental programs", Nuclear Engineering and Design, Vol. 237, 2007, pp. 1872-1886.
- [2] A. Guelfi, D. Bestion, M. Boucker, P. Boudier, P. Fillion, M. Grandotto, J-M. Hérard, E. Hervieu, P. Péturaud, "NEPTUNE A new software platform for advanced nuclear thermal hydraulics", Nuclear Science and Engineering, vol. 156, 2007, pp. 281-324.
- [3] M. Boucker, A. Guelfi, S. Mimouni, P. Péturaud, D. Bestion, E. Hervieu, "Towards the prediction of local thermalhydraulics in real PWR core conditions unsing NEPTUNE\_CFD software", Workshop on modeling and Measurements of two-Phase Flows and Heat transfer in Nuclear Fuel Assemblies, KTH, Stockholm, Sweden -10-11 October, 2006.
- [4] D.M. Newitt, N. Dombrowski et F.H. Knelman: Liquid entrainment: 1. the mechanism of drop formation from gas and vapour bubbles. Trans. Instn Chem. Engrs, 32:244–261, 1954.
- [5] M. Andreani, "Studies of Dispersed Flow Film Boiling with 3-D Lagrangian Hydrodynamics and a 2-D Eulerian Vapour Field", PhD Thesis, Swiss Federal Institut of Technology Zurich, 1992.
- [6] T.R. Auton, "The lift force on a spherical body in a rotational flow", J. Fluid Mech. 183 (1987), pp. 190–218.
- [7] D. Baalbaki, A. Toutant, P. Ruyer and F. Bataille, "Modeling and Simulation of turbulent and non-isothermal two-phase flow", 7<sup>th</sup> International Conference on Multiphase Flow, ICMF 2010, Tampa, Florida, May 30-June 4, 2010.
- [8] P.W. Saffman, "The lift on a small sphere in a slow shear flow, Journal of Fluid Mechanics, vol. 22, 1965, 1385-1400".
- [9] P. Kurose, R. Misumi, S. Komori, "Drag and lift Forces acting on a spherical bubble in a linear shear flow", International Journal of Multiphase Flow, vol. 27, 2001, pp. 1247-1258.
- [10] K-I Sugioka, S. Komori, "Drag and lift Forces acting on a spherical water droplet in homogeneous linear shear air flow", J. Fluid Mech., vol. 570, 2007, pp. 155-175.
- [11] W.P. Jones and B.E Launder, "The prediction of laminarization with a two-equation model of turbulence. International Journal of Heat and Mass Transfer", vol. 15, 1972, pp. 301-14.
- [12] J.O. Hinze, "Turbulence". McGraw-Hill College, 1975.
- [13] L.X. Zhou, "Advances in studies on two-phase turbulence in dispersed multiphase flows". Int. J. Multiphase Flow, vol. 36, 2010, pp. 100–108.
- [14] E.N. Ganic, W.M. Rohsenow, "On the mechanism of liquid drop deposition in two-phase dispersed flow". Journal of Heat Transfer, vol. 101, 1979, pp.288–296.

- [15] M. Andreani, G. Yadigaroglu, "A 3-D Eulerian-Lagrangian model of dispersed flow film boiling including a mechanistic description of the droplet spectrum evolution I. The thermalhydraulic model. Int. J. Heat and Mass Transfer, vol. 40 (suppl. 8), 1997, pp. 1753-1772.
- [16] G. Castanet, F. Lemoine "Heat transfer within combusting droplets. Proceedings of the Combustion Institute, 2007.
- [17] B. Abramzon, S. Sahzin "Convective vaporization of a fuel droplet with thermal radiation" absorption. Fuel, vol. 85, 2006, pp. 32–46.
- [18] M. Hendou, "Contribution à la modélisation des transferts simultanés lors de l'absorption de gaz tracés par une pulverisation". Thèse de doctorat, ENSIGC, 1992.
- [19] G.M. Harpole, "Water droplet evaporation in high temperature surrounds". Rapport technique, ASME paper 79-WA/HT-6, 1979.
- [20] M.C. Yuen, L.W. Chen, "Heat transfer measurements of evaporating liquid droplets", International Journal of Heat and Mass Transfer, 21:537–542, 1973.
- [21] R. Lee, J.N. Reyes et K. Almenas, "Size and number density change of droplet populations above the quench front during reflood". International Journal of Heat and Mass Transfer, vol. 27, 1984, pp. 573-585.
- [22] M. Gradeck, D. Maillet, F. Lelong, N. Seiler, G. Repetto, "Estimation of droplets/wall heat transfer under LOCA conditions in a PWR", La Houille Blanche, Internationale Revue de l'eau, 4 (2009) 65-71, doi 101051/lhb/2009046.
- [23] F. Lelong, M. Gradeck, D. Maillet, N. Seiler, "Experimental study of heat transfer between droplets and wall in Leidenfrost regime", 7th Int. Conference on Multiphase Flow (ICMF), Tampa, FL USA, May 30-June 4, 2010.
- [24] F. Lelong, M. Gradeck, N. Seiler, G. Castanet, P. Dunand "Behaviour of liquid droplets bouncing onto a hot slab", ILASS- Europe 2010, 23<sup>rd</sup> Annual conference on Liquid Atomization and Spray System, Brno, Czech Republic, September 2010.
- [25] C. Morel, P. Ruyer, N. Seiler, J. Laviéville, "Comparison of several models of multisize bubbly flows on an adiabatic experiment", International Journal of Multiphase Flow, vol. 36 (suppl. 1), 2008, pp. 25-39.
- [26] P.J. O'Rourke, A.A. Amsden, T.D. Butler. "Kiva-ii: a computer program for chemically reactive flows with sprays". Technical report, Los Alamos, LA-11560-MS, 1989.
- [27] H.S. Aly, Y.A. Eldrainy, K.M. Saqr, T.M. Lazim, M.N.M. Jaafar "A mathematical model for predicting spray atomization characteristics in an Eulerian-Eulerian framework". International communications in heat and mass transfer, vol. 37, 2010, pp. 618–623, 2010.
- [28] N.I. Kolev. "Multiphase Flow Dynamics II: Thermal and Mechanical Interactions". Springer Berlin Heidelberg, 2005.
- [29] R.R. Schroder, R.C. Kitner. "Oscillation of a drop falling in liquid field". A.I.Ch.E. Journal, vol. 11, 1965, pp.5–8.

[30] N. Seiler, P. Ruyer, "Evaluation of contribution from the radiative heat in dispersed flow configuration during the reflooding phase of LOCA" NURISP (NUclear Reactor Integrated Simulation Project) Seventh Framework Programme EURATOM, 232124, Deliverable D2.4.3.21a.